Can core-surface flow models be used to improve the forecast of the Earth's main magnetic field?

Stefan Maus, Luis Silva, Gauthier Hulot

Can core-surface flow models be used to improve the forecast of the Earth's main magnetic field?

Stefan Maus,[1,2,3] Luis Silva,[3] and Gauthier Hulot[3]

Received 1 June 2007; revised 22 May 2008; accepted 3 June 2008; published 13 August 2008.

[1] Geomagnetic main field models used for navigation are updated every 5 years and contain a forecast of the geomagnetic secular variation for the upcoming epoch. Forecasting secular variation is a difficult task. The change of the main magnetic field is thought to be principally due to advection of the field by flow at the surface of the outer core on short timescales and when large length scales are considered. With accurate secular variation (SV) and secular acceleration (SA) models now available from new satellite missions, inverting for the flow and advecting it forward could lead to a more accurate prediction of the main field. However, this scheme faces two significant challenges. The first arises from the truncation of the observable main field at spherical harmonic degree 13. This can however be handled if the true core flow is large scale and has a rapidly decaying energy spectrum. The second is that even at a given single epoch the instantaneous SV and SA cannot simultaneously be explained by a steady flow. Nevertheless, we find that it may be feasible to use flow models for an improved temporal extrapolation of the main field. A medium-term ($\approx$10 years) hindcast of the field using a steady flow model outperforms the usual extrapolation using the presently observed SV and SA. On the other hand, our accelerated, toroidal flow model, which explains a larger portion of the observed average SA over the 2000–2005 period, fails to improve both the short-term and medium-term hindcasts of the field. This somewhat paradoxical result is related to the occurrence of so-called geomagnetic jerks, the still poorly known dynamical nature of which remains the main obstacle to improved geomagnetic field forecasts.

Citation: Maus, S., L. Silva, and G. Hulot (2008), Can core-surface flow models be used to improve the forecast of the Earth's main magnetic field?, *J. Geophys. Res.*, *113*, B08102, doi:10.1029/2007JB005199.

1. Introduction

[2] An important practical application of geomagnetic field research is the production of main field models for navigation and pointing (e.g., for directional drilling). The most widely used models are the International Geomagnetic Reference Field (IGRF) [*Maus et al.*, 2005b] and the World Magnetic Model (WMM) [*McLean et al.*, 2004]. Both models are spherical harmonic representations of the main magnetic field up to spherical harmonic degree 13 and 12, respectively. The models are updated in 5-year intervals and include the predicted first time derivative of the coefficients up to degree 8 for the upcoming epoch. The accuracy of these predictions for the past decades, as inferred from our retrospective knowledge of the field, is illustrated in Figure 1.

[3] New satellite magnetic missions, Ørsted (since 1999), Challenging Minisatellite Payload for Geophysical Research and Application (CHAMP) (since 2000), and SAC-C (2001–2004), have monitored the geomagnetic field over the past 9 years. On the basis of an excellent data coverage, the IGRF and WMM models for 2000 and 2005 have been more accurate than ever before, with estimated errors of the order of 10 nT for the main field at the Earth's surface for the starting dates of the models [*Maus et al.*, 2005a]. In contrast, the prediction of the secular variation for the upcoming epoch has not seen a comparable improvement. The expected error at the end of the 5 year validity of these models is still of the order of 100 nT [*Maus et al.*, 2005a]. The aim of the present study is therefore to find ways of improving the forecast of the magnetic field. For that purpose we investigate the effectiveness of using core flow models.

[4] From the new satellite data, the first and second time derivatives of the main magnetic field, referred to here as secular variation (SV) and secular acceleration (SA), can be inferred with unprecedented accuracy [*Maus et al.*, 2006; *Olsen et al.*, 2006]. The change of the main magnetic field on timescales of a decade or less is thought to be principally due to advection of the field by flow at the top of the outer core [*Roberts and Scott*, 1965]. Numerous studies have shown that MF and SV models for a given epoch can be used to infer the core-surface flow for that same epoch [*Bloxham and Jackson*, 1991; *Hulot et al.*, 2002; *Holme and*

[1]CIRES, University of Colorado, Boulder, Colorado, USA.
[2]National Geophysical Data Center, NOAA E/GC1, Boulder, Colorado, USA.
[3]Equipe de Géomagnétisme, Institut de Physique du Globe de Paris, INSU/CNRS, Université Paris Diderot, Paris, France.

0148-0227/08/2007JB005199$09.00

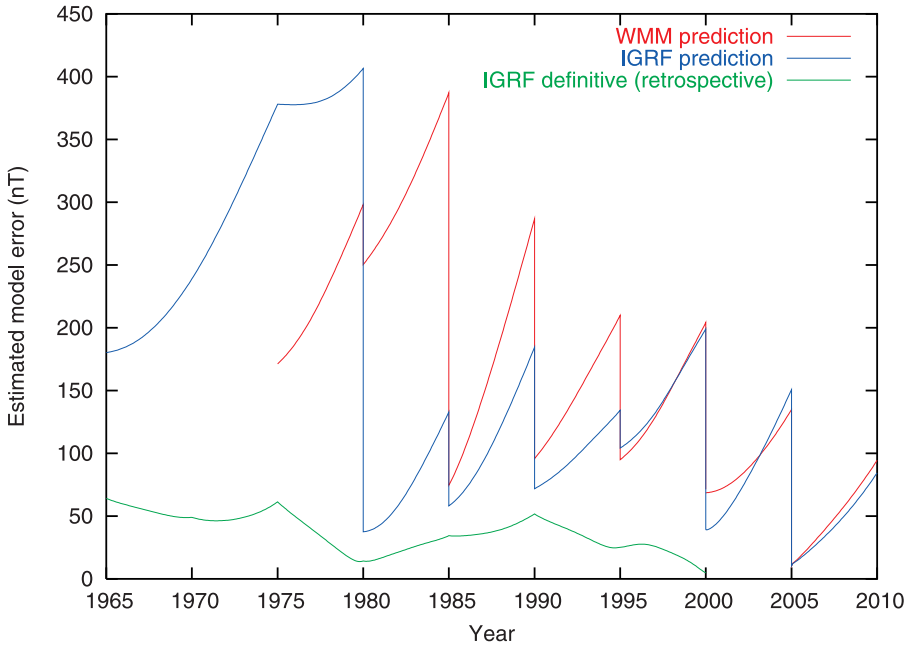

Figure 1. Main field errors of the WMM and the predictive and retrospective models of the IGRF, as estimated from the misfit, defined in equation (16), with the main field Comprehensive Model (CM4) [*Sabaka et al.*, 2004] for 1965–2000 and the model Pomme-3.0 [*Maus et al.*, 2006] for 2000–2010. One can see the strong influence of the satellite missions Magsat (winter 1979–1980) and Ørsted/CHAMP/SAC-C (1999 to present). The WMM is a model that is produced on time, before the start of the upcoming epoch. Therefore the WMM-1980 missed the Magsat data and the WMM-2000 missed the vector data from Ørsted, explaining the larger model errors in comparison with the IGRF. While the WMM is strictly an operational model for the present, the IGRF is updated retrospectively to include a definitive model for the past, whose misfit is also displayed here.

Olsen, 2006]. But the results are ambiguous [see, e.g., *Eymin and Hulot*, 2005] and with the increased resolution of the new satellite data, stronger medium and small-scale flows have to be invoked [*Hulot et al.*, 2002; *Voorhies*, 2004]. Making use of the SA for the same epoch however brings additional information. This information can be used to also infer an estimate of the flow acceleration and to reduce the flow ambiguity if the form of the flow acceleration is constrained by dynamical considerations. Because core flows are intrinsically the physical cause of the SV, relying on such estimates at a given initial epoch to produce an order 1 Taylor expansion of the flow, might then provide a better means of predicting the magnetic field, than a simple extrapolation of an order 2 Taylor expansion of the field itself, at least over the time period over which we may hope core dynamics to keep the flow acceleration essentially constant. This is what the present study intends to test.

[5] Here, we therefore build simple instantaneous core flow and flow acceleration estimates that account for the 2003.0 SV and SA as provided by POMME3.0, a main field model which describes the field evolution in terms of an order 2 Taylor expansion (i.e., with constant SA) over the 2000.5–2005.5 time period [*Maus et al.*, 2006]. We first look for a steady flow that accounts for the 2003.0 SV and SA, since the steady flow assumption removes part of the ambiguity in flow inversions [*Voorhies and Backus*, 1985]. We show however that such a steady flow cannot account for the large amplitude of the POMME3.0 SA, even if no additional constraints such as geostrophy or toroidal flow are imposed. This is consistent with earlier studies, e.g., by *Waddington et al.* [1995], who found that steady flow models are not able to explain the long-term SA found in the historical observatory data. We therefore next compute a flow with a zonal flow acceleration. This allows us to explain a slightly larger portion of the 2003.0 SA. However, explaining most of this SA clearly requires a generally accelerated flow. In a third set of calculations we therefore tentatively compute a flow together with a more general acceleration, but restrict both to be toroidal in order to avoid further nonuniqueness issues. Finally, to investigate whether any of these flow and acceleration models for epoch 2003.0 could indeed help in providing a more accurate forecast of the geomagnetic field, we backward extrapolate the flow (as an order 1 Taylor expansion based on the 2003.0 flow and flow acceleration), use this extrapolation to hindcast the field according to the induction equation, and compare this hindcast with the main field independently given by the Comprehensive Model [*Sabaka et al.*, 2004].

2. Core Flow Inversion

[6] The Earth's core field, of which we can only observe the poloidal part, is completely determined by the radial component of the magnetic field at the core-mantle boundary (assuming negligible mantle conductivity). Here, we first describe our scheme of inverting magnetic field observations for flows at the surface of the outer core.

2.1. Magnetic Field Observations

[7] For this study, we use geomagnetic field models which provide concise representations of the observed magnetic field and its temporal derivatives in terms of truncated spherical harmonic expansions. Because of the uneven distribution of magnetic observatories, geomagnetic field models estimated from observatory data only are not reliable for spherical harmonic coefficients with a degree higher than seven [*Alexandrescu et al.*, 1994]. The changing distribution of observatories adds additional uncertainties in the SV and SA estimates [*Alexandrescu et al.*, 1994]. Since 1999 however, and thanks to the present generation of low orbiting magnetic satellites, the situation very significantly improved and accurate estimates of the SV and SA to spherical harmonic degree 13 and higher can now be recovered [*Maus et al.*, 2006; *Olsen et al.*, 2006; *Hulot et al.*, 2007]. Because of the short time lapse since 1999 a simple Taylor series expansion of the field around a center epoch (2003.0 for POMME-3) can be considered. This is the model we use to derive an instantaneous estimate of the flow and acceleration at the same epoch. Of course, once longer time series of satellite data are available, it will always be possible to use field models parametrized by cubic B-splines, as in historic field models such as UFM [*Bloxham and Jackson*, 1992], to infer continuously time-varying flows as done by, e.g., *Jackson* [1997] and *Holme* [1998]. Note however that for the purpose of investigating the forecasting power of stationary or constantly accelerated flows over some period of time, the present approach is already fully appropriate.

[8] For magnetic field variations longer than a couple of years, the mantle can be considered as an electrical insulator [*Backus et al.*, 1996; *Alexandrescu et al.*, 1999]. The magnetic field and its temporal variations at the core-mantle boundary can thus be directly inferred from geomagnetic field models, with the important limitation that the core field is masked by the crustal field starting from spherical harmonic degree 14 [*Langel and Hinze*, 1998]. Since the crustal field can reasonably be assumed static, this means that the core field cannot be known beyond degree 13, except for its time change. Those can then be used to higher degrees, keeping in mind, however, that the signal is very weak at these high degrees, and thus much less constrained. Formally, we will therefore use the main field to degree 13, and the SV and SA to degree 16 for epoch 2003.0 as given by POMME3.0 (the Potsdam Magnetic Model of the Earth (POMME), version 3.0 [*Maus et al.*, 2006]). However, for reasons that are explained later, we will not attempt to account for the small scales of the SV and SA beyond respectively degrees 9 and 6.

2.2. Induction Equation

[9] The radial component of the magnetic field is related to the flow $\mathbf{u}$ at the top of the core by the induction equation [see, e.g., *Jackson and Finlay*, 2007]

$$\dot{B}_r = \underbrace{-\nabla_H \cdot \mathbf{u} B_r}_{\text{advection}} + \underbrace{\frac{\eta}{r}\nabla^2 r B_r}_{\text{diffusion}} \tag{1}$$

$$\dot{B}_r = -B_r \nabla_H \cdot \mathbf{u} - \mathbf{u} \cdot \nabla_H B_r + \frac{\eta}{r}\nabla^2 r B_r, \tag{2}$$

where $\nabla_H = \nabla - \hat{\mathbf{r}}\partial_r$ is the horizontal part of the gradient. The new geomagnetic field models also provide additional information on the second time derivative of the field (SA), which is related to the flow by

$$\ddot{B}_r = -\dot{B}_r \nabla_H \cdot \mathbf{u} - B_r \nabla_H \cdot \dot{\mathbf{u}} - \dot{\mathbf{u}} \cdot \nabla_H B_r - \mathbf{u} \cdot \nabla_H \dot{B}_r + \frac{\eta}{r}\nabla^2 r \dot{B}_r. \tag{3}$$

On timescales of about 5 years considered here, the advection term is thought to strongly dominate over diffusion [*Jackson and Finlay*, 2007]. We therefore assume the frozen flux condition [*Roberts and Scott*, 1965] and drop the diffusion terms in (1)–(3).

2.3. Parameterization of the Flow

[10] Several parameterizations are used in this study to represent the flow.

2.3.1. General Flow

[11] At the start of this study we allow for a general flow, where the flow components are expressed in the usual poloidal-toroidal representation [*Eymin and Hulot*, 2005]

$$u_\vartheta(\vartheta,\varphi) = \sum_{\ell=1}^{N}\sum_{m=-\ell}^{\ell}\left(s_\ell^m \partial_\vartheta \beta_\ell^m(\vartheta,\varphi) + \frac{t_\ell^m}{\sin\vartheta}\partial_\varphi \beta_\ell^m(\vartheta,\varphi)\right) \tag{4}$$

$$u_\varphi(\vartheta,\varphi) = \sum_{\ell=1}^{N}\sum_{m=-\ell}^{\ell}\left(\frac{s_\ell^m}{\sin\vartheta}\partial_\varphi \beta_\ell^m(\vartheta,\varphi) - t_\ell^m \partial_\vartheta \beta_\ell^m(\vartheta,\varphi)\right), \tag{5}$$

where β_ℓ^m are Schmidt seminormalized spherical harmonics [*Backus et al.*, 1996], and s_ℓ^m and t_ℓ^m are the poloidal and toroidal coefficients of the flow, respectively.

2.3.2. Zonal Acceleration

[12] Work by *Braginsky* [1970] and *Jault et al.* [1988, 1996] and more recently *Zatman and Bloxham* [1999], *Bloxham et al.* [2002], and *Mound and Buffett* [2005] has shown that torsional oscillations likely play an important role in the dynamics of the core on timescales of years to decades. Torsional oscillations consist of zonal accelerations of the flow in the φ direction. Assuming that the period of the oscillations significantly exceeds the time frame of about 5 years considered here, we merely model a constant acceleration of the flow in the longitudinal direction, rather than a full oscillation with a period and a phase. The acceleration is parameterized by taking the first time derivative of (5) for toroidal zonal flow, leading to

$$\dot{u}_\varphi(\vartheta) = -\sum_{\ell=1}^{N} \dot{t}_\ell^0 \partial_\vartheta \beta_\ell^0(\vartheta), \tag{6}$$

with no dependence on the longitude φ.

2.3.3. Toroidal Flow

[13] Finding a flow that explains the observed change in the radial component of the magnetic field at the core-mantle boundary is an underdetermined problem, in the sense that different core flows can explain the observations equally well [*Backus*, 1968]. In order to reduce the number of unknown parameters, one can impose physical constraints on the flow. Commonly used constraints are that

the flow is tangentially geostrophic [*LeMouël*, 1984] or toroidal [*Whaler*, 1980]. A toroidal representation of the flow velocity follows from (4) and (5) for $s_\ell^m = 0$ as

$$u_\vartheta(\vartheta,\varphi) = \sum_{\ell=1}^{N}\sum_{m=-\ell}^{\ell} \frac{t_\ell^m}{\sin\vartheta}\partial_\varphi \beta_\ell^m(\vartheta,\varphi) \tag{7}$$

$$u_\varphi(\vartheta,\varphi) = -\sum_{\ell=1}^{N}\sum_{m=-\ell}^{\ell} t_\ell^m \partial_\vartheta \beta_\ell^m(\vartheta,\varphi). \tag{8}$$

A corresponding representation of the flow acceleration is obtained by taking the first time derivative of u_ϑ and u_φ, and introducing coefficients $\dot{t}_\ell^m$.

2.4. Numerical Implementation

[14] To invert for core-surface flow, one must insert the desired flow parameterizations of (4) to (8) into the two induction equations (2) and (3). The resulting system of equations can be solved as a generalized least squares problem [*Menke*, 1984; *Gubbins and Bloxham*, 1985]

$$(A^T C_{obs}^{-1} A + \lambda C_u^{-1})\mathbf{m} = A^T C_{obs}^{-1}\mathbf{d}. \tag{9}$$

Here, $\mathbf{m}$ is the vector of unknown model parameters. Depending on the assumptions used, $\mathbf{m}$ thus consists of various combinations of poloidal s_ℓ^m and toroidal t_ℓ^m flow coefficients, and zonal $\dot{t}_\ell^0$ and toroidal $\dot{t}_\ell^m$ flow acceleration coefficients. Then, A is a matrix giving the effect of a unit perturbation in one of the model parameters on the vector of observations $\mathbf{d}$, C_{obs} is the covariance matrix of the observations and λC_u^{-1} is the damping imposed on the solution. The vector of observations consists of the observed spherical harmonic coefficients of the SV and SA. To find the matrix A, one has to know the contribution of a given flow model parameter of degree ℓ and order m to each element of $\mathbf{d}$. This is not trivial because the equations include spatial derivatives which change the spherical harmonic degree and order of the terms [see, e.g., *Hulot et al.*, 1992].

[15] To avoid extensive analytical considerations, we numerically generate the matrix A by synthesizing the two induction equations (2) and (3) on an equal area spatial grid, numerically approximate the spatial derivatives, and then multiply the grid with the spherical harmonic basis functions to transform it back into the spectral domain. Let us illustrate the procedure on a simple example, namely, solving the first induction equation (2) for toroidal flow (with the diffusion terms dropped). In this case, the terms containing the divergence of the flow are zero and the equation reduces to

$$u_\vartheta \frac{1}{r}\partial_\vartheta B_r + u_\varphi \frac{1}{r\sin\vartheta}\partial_\varphi B_r = -\dot{B}_r. \tag{10}$$

Inserting the toroidal flow parametrization (7) and (8) gives

$$\sum_{\ell',m'} t_{\ell'}^{m'} \frac{1}{\sin\vartheta}(\partial_\varphi \beta_{\ell'}^{m'})\frac{1}{r}\partial_\vartheta B_r - \sum_{\ell',m'} t_{\ell'}^{m'}(\partial_\vartheta \beta_{\ell'}^{m'})\frac{1}{r\sin\vartheta}\partial_\varphi B_r = -\dot{B}_r. \tag{11}$$

The corresponding equation of degree ℓ and order m in the spectral domain is obtained by (1) synthesizing the values on an equal area grid (ϑ_i, φ_i), (2) multiplying by $\beta_\ell^m(\vartheta_i, \varphi_i)$, (3) summing over all i and (4) normalizing by dividing by $\sum_i[\beta_\ell^m(\vartheta_i, \varphi_i)]^2$. If we denote this transform by $\int_S \cdot\, \beta_\ell^m dS$, we get one equation for each degree ℓ and order m as

$$\sum_{\ell',m'} t_{\ell'}^{m'} \int_S \frac{1}{r\sin\vartheta}\left[(\partial_\varphi \beta_{\ell'}^{m'})\partial_\vartheta B_r - (\partial_\vartheta \beta_{\ell'}^{m'})\partial_\varphi B_r\right]\beta_\ell^m dS = -(\dot{B}_r)_\ell^m. \tag{12}$$

Here, the coefficients $(B_r)_\ell^m$ and $(\dot{B}_r)_\ell^m$ of the observed radial field are directly obtained from the Gauss coefficients g_ℓ^m and $\dot{g}_\ell^m$, as given by

$$(B_r)_\ell^m = (\ell+1)\left(\frac{R_E}{R_C}\right)^{\ell+2} g_\ell^m, \tag{13}$$

where R_E and R_C are the radius of the Earth and core, respectively. Equation (12) corresponds to one row of the matrix A, relating the entire model vector of toroidal flow coefficients $t_{\ell'}^{m'}$ to one SV coefficient $\dot{g}_\ell^m$. If the SV is used up to degree N, this gives $N(N+2)$ such rows of A. In addition, the SA yields a corresponding number of rows, resulting in a total of $2N(N+2)$.

2.5. Data Weighting and Regularization

[16] Following *Pais and Hulot* [2000], we use a covariance matrix which minimizes the residual SV energy at the Earth's surface and is given by

$$C_{SV}^{-1} = \frac{1}{W_{SV}(\ell+1)}\left(\frac{R_C}{R_E}\right)^{2\ell+4} I, \tag{14}$$

where W_{SV} is a scaling parameter with unit $(\mathrm{nT/a})^2$ (where a is years) and I is the identity matrix. The same covariance matrix with a corresponding scaling parameter W_{SA} is used for the SA. For the regularization we follow the same work [*Pais and Hulot*, 2000], using

$$\lambda C_u^{-1} = \lambda E^{-1}\ell^{p+1}(\ell+1)I, \tag{15}$$

where λ is a dimensionless damping parameter, while E is a second scaling parameter with units $(\mathrm{km/a})^2$. The parameter p is the exponent of the desired decrease of the velocity spectrum of the flow. As the limiting case, the spectrum must decay faster than ℓ^{-1}, corresponding to $p = 1$, in order to have finite kinetic energy [*Hulot et al.*, 1992]. *Pais and Hulot* [2000] and *Eymin and Hulot* [2005] used a value of $p = 3$. It should however be noted that the term in (15) does not necessarily enforce the desired decay in the energy spectrum. The effect of the regularization depends on the actual coefficients of the matrix A and therefore cannot easily be guessed *a priori*. The result of the regularization therefore has to be verified by plotting the resulting flow spectrum and then varying the regularization, possibly using extensions of (15), until the desired spectrum is enforced. By trial and error we choose the weakest regularization leading to an a posteriori $p = 3$ decay in the flow velocity

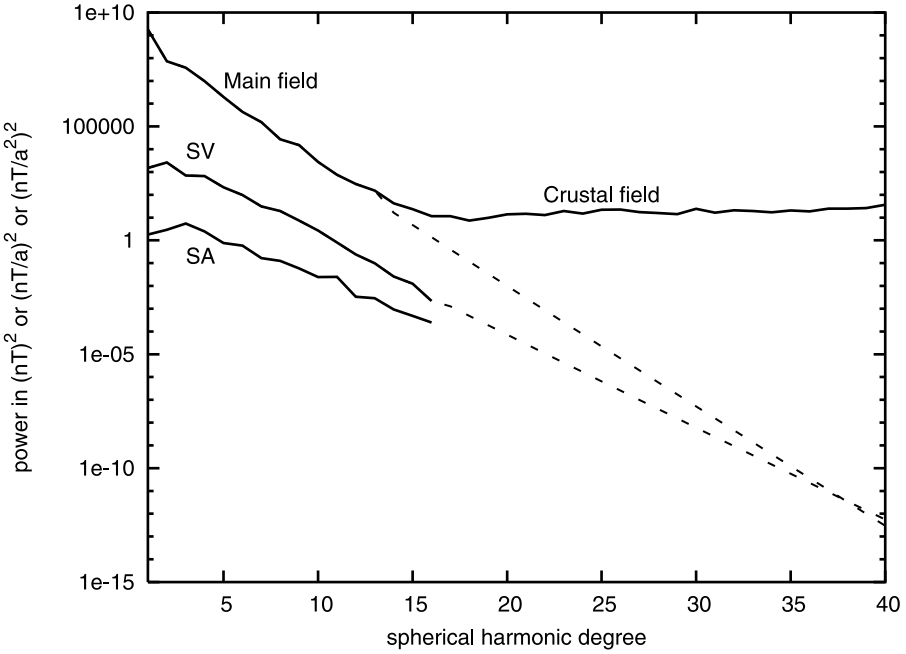

Figure 2. Mauersberger/Lowes spectra at the Earth's surface of the main field, secular variation (SV), and secular acceleration (SA), together with their random extensions, to be used for self-consistency checks. The main field model was in fact extended further to degree 90, while the SV spectrum was only extended to degree 40, assuming that higher-degree SV would have timescales that are too short to be relevant here.

and acceleration spectra (comparable to those used by *Eymin and Hulot* [2005]).

2.6. Truncation Effects and Self-Consistency

[17] As pointed out by *Hulot et al.* [1992], the low-degree part of a truncated flow solution interacts with the unknown high-degree main field to create additional low-degree SV. In addition, the true flow extends beyond our truncated solution. Interaction of the unknown high-degree flow with the main field generates additional large-scale SV. The same reasoning holds for the truncation of the SV and the flow acceleration, and the resultant additional SA. A solution can only be considered as self-consistent if the additional SV and SA can be accommodated for either by SV and SA uncertainties, or by unmodeled SV and SA. Otherwise the solution is self-contradicting. In an effort to take this effect into account, we adopt the strategy of *Eymin and Hulot* [2005], and rely on random extensions of the spectra of the main field, the SV, the flow velocity and the flow acceleration (which we note, is a reasonable but rough assumption, since the true small-scale field and flow are not random, and diffusion is ignored). The resulting interactions lead to additional contributions to the SV and SA, which must be smaller than the unmodeled SV and SA. We carry out this test extending the main field to spherical harmonic degree 90 and the SV to degree 40 (see Figure 2). The main field degree was chosen arbitrarily, while the SV was truncated at degree 40 where the annual change starts to exceed the strength of the field. The flow velocity and flow acceleration are also randomly extended to degree 40, which is high enough to investigate the effects of the leading terms on the observed field [*Eymin and Hulot*, 2005]. As we shall later see, the resulting interactions show that the demand for self-consistency poses serious limitations on core-surface flow modeling.

3. Results

[18] This section describes the ability of the resulting flow solutions to represent the 2003.0 SV and SA and their quality for forecasting or hindcasting the field. We formally invert for the flow velocity (and its acceleration, where applicable) to degree 16. In all inversions we use the covariance matrix as given by (14), accordingly down-weighting the high-degree observations of the SV and SA.

3.1. Steady Flow

[19] Considering the 2003.0 SV and SA as complementary observations, our first attempt is to explain both of these observations simultaneously by a steady flow. In other words, we invert for a flow which simultaneously explains the SV and SA as a result of respectively advecting the main field and the SV. We use the classical representation of equations (4) and (5) for the u_ϑ and u_φ components of the flow. No further constraints are imposed.

[20] First, we invert with no damping of the flow. Not surprisingly, we find that an unconstrained flow to degree 16 can completely reproduce both the SV and the SA to degree 16. However, the resulting flow has unreasonable velocities up to several thousand kilometers per year. Its spectrum increases with degree, meaning that the truncated solution is meaningless because the (unmodeled) small scales of the flow would overshadow the effect of the (modeled) larger scales.

[21] A better behaved solution is obtained when the flow is damped using the regularization given in (15). The steady

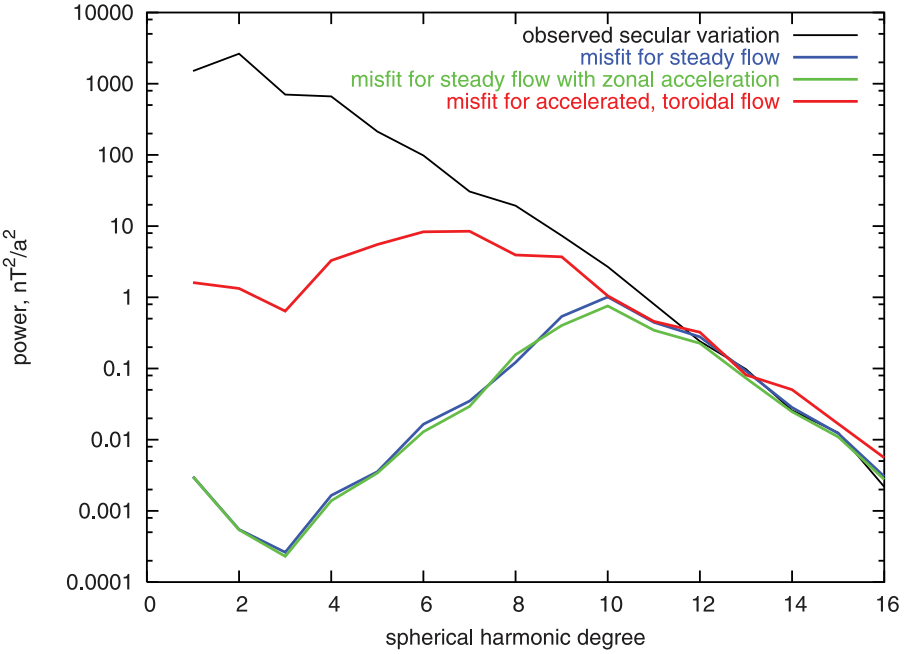

Figure 3. Mauersberger/Lowes spectrum of the SV at the Earth's surface, together with the difference spectra between the observed SV and the one explained by the different flow models. Forcing the flow to be toroidal decreases its ability to completely explain the SV. However, this is of limited significance since truncation effects overshadow this effect, as shown in Figure 7a below.

flow solution is shown in Figure 5a and its component velocity spectra in Figure 6a. Figure 3 (red curve) shows that the damped flow still explains the SV well up to spherical harmonic degree 9. However, it fails to explain most of the observed SA (Figure 4). Forcing the steady flow to better explain the SA by changing the relative weights of W_{SV} and W_{SA} is possible. But for the flow to keep a well-behaved spectrum, this can only be done at the expense of much relaxing the fit to the SV. This means that a flow that explains the SV at a satisfactory level (i.e., in a self-consistent way, see below) by advecting the main field, cannot at the same time explain the SA by advecting the SV.

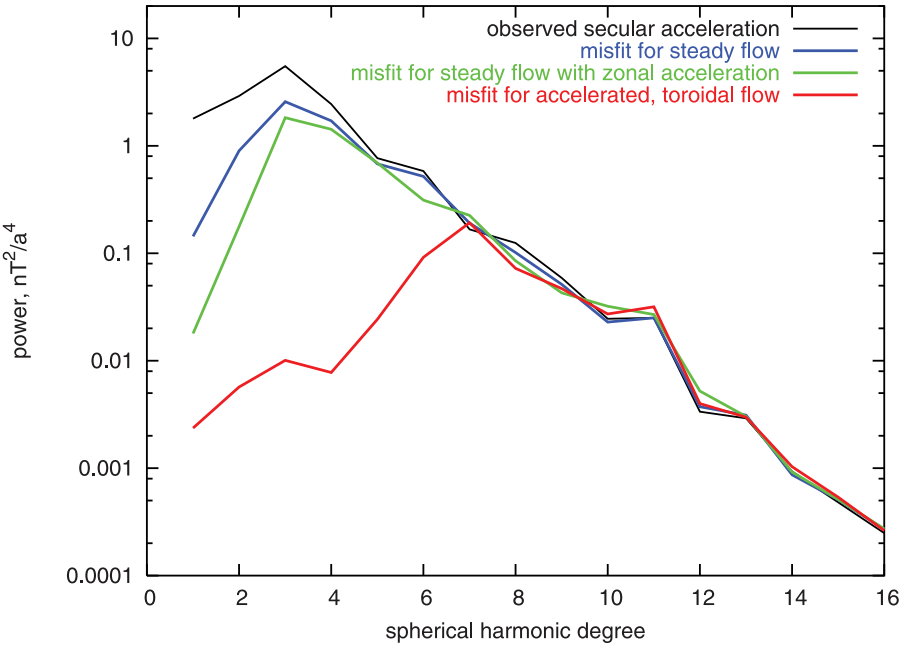

Figure 4. Same as Figure 3 but for the SA. Only a small part of the SA can be explained by steady flow. A significant improvement results from allowing for zonal flow acceleration. However, a more complete representation of the SA requires a fully accelerated flow.

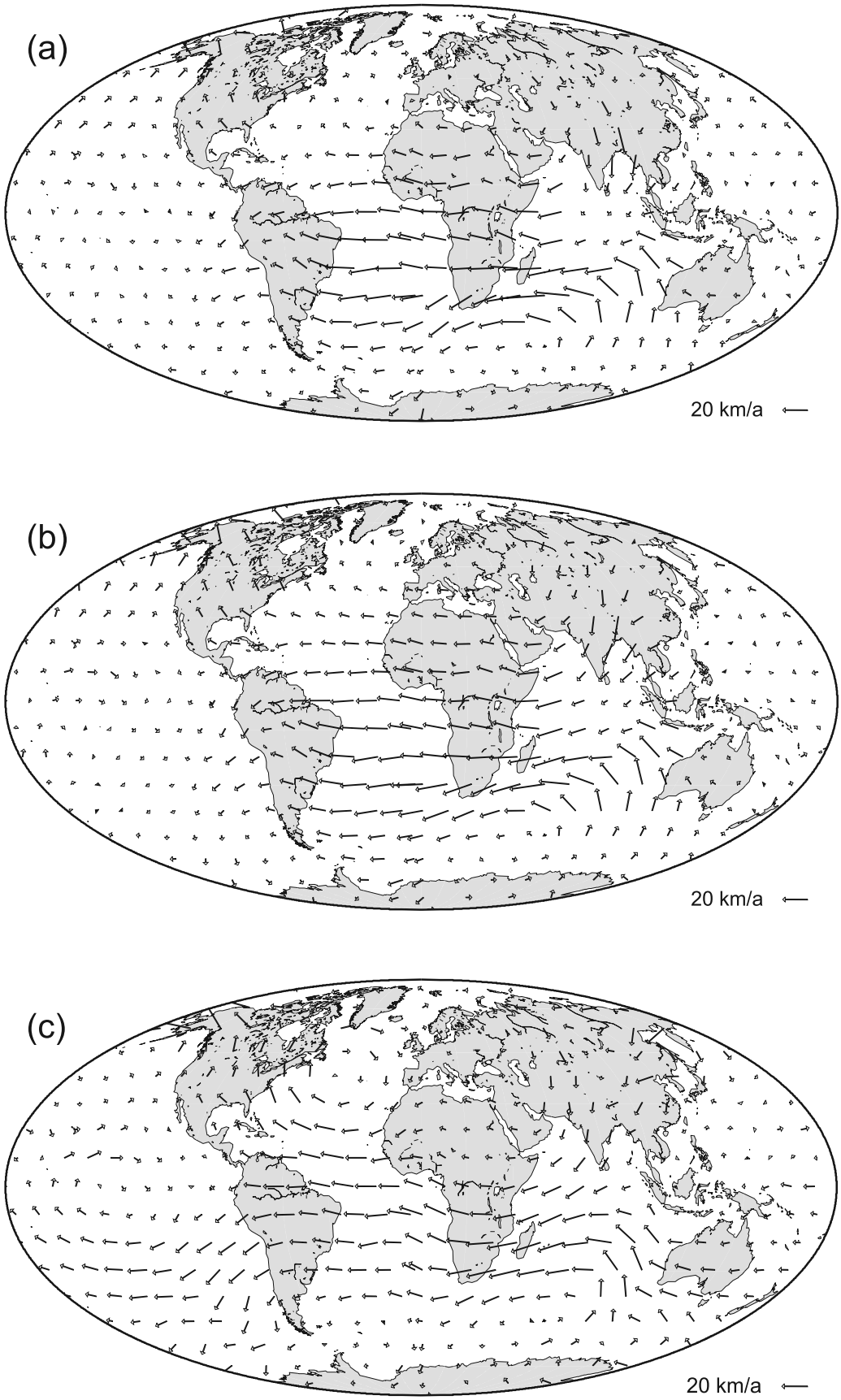

Figure 5. Velocity vectors of the solutions for (a) steady flow, (b) steady flow with zonal acceleration, and (c) accelerated toroidal flow. Arrows are centered on the balance point. Overall, velocities decrease from Figure 5a over Figure 5b to Figure 5c.

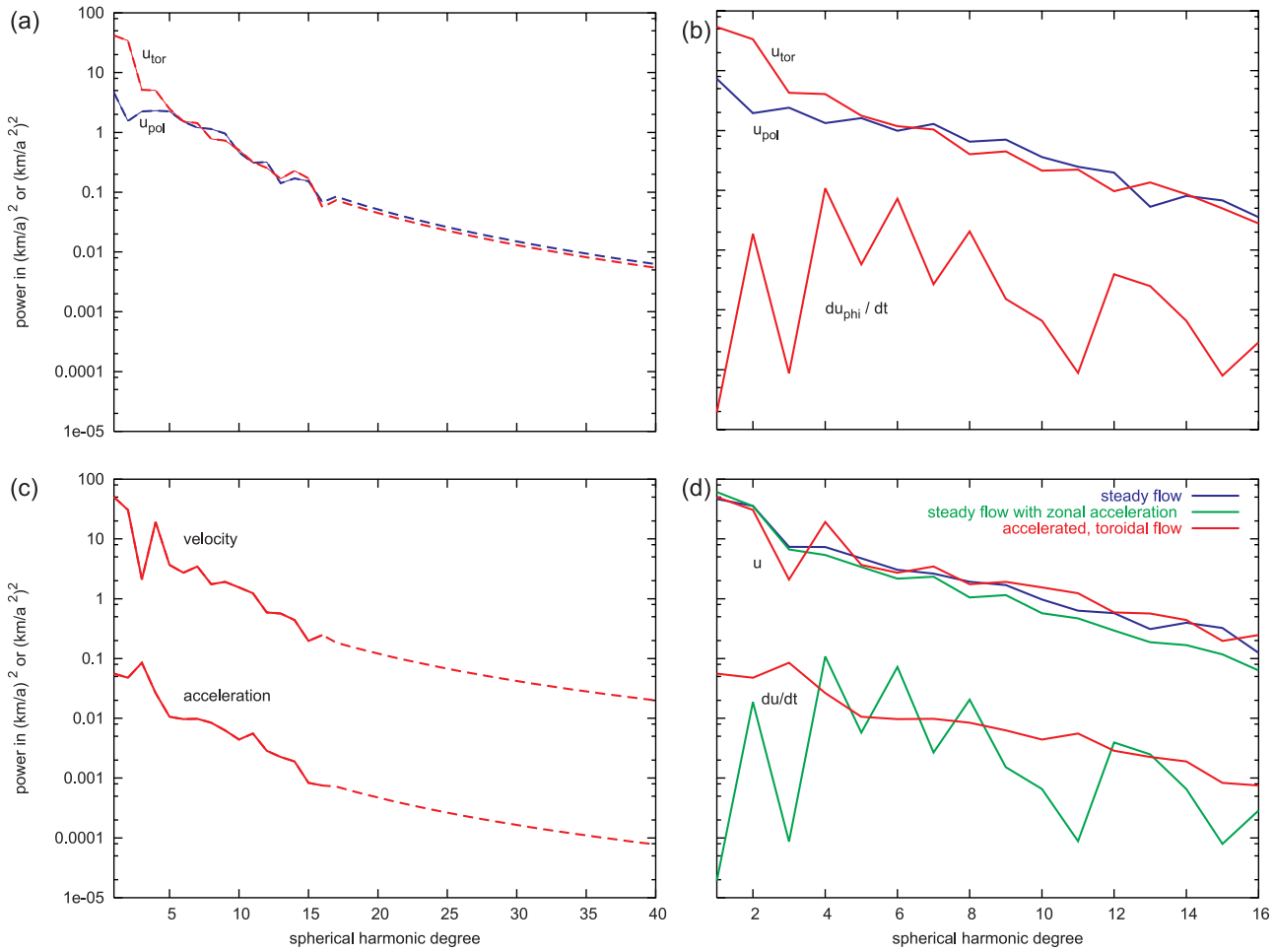

Figure 6. Velocity and acceleration spectra for (a) steady flow, (b) steady flow with zonal acceleration, and (c) accelerated toroidal flow. (d) A comparison of the spectra for these three different cases. The spectra in Figures 6a and 6b are computed as $E(\ell) = 1/(2\ell + 1)\sum_m (u_\ell^m)^2$, where the factor $1/(2\ell + 1)$ is due to Schmidt's seminormalization. The spectra of toroidal flow in Figure 6c are computed as $E(\ell) = \ell(\ell + 1)/(2\ell + 1)\sum_m (t_\ell^m)^2$, following the derivation of *Hulot et al.* [1992]. For Figure 6d the spectra of u_φ and u_ϑ were combined to a total velocity as $E(\ell) = 1/(2\ell + 1)\sum_m (u_\ell^m)^2 + (v_\ell^m)^2$. The dashed lines in Figures 6a and 6c show the extended coefficients, using rescaled random numbers. These random extensions are used to test the self-consistency of the flow solutions.

This, in fact, is not surprising because the SV per year is typically 3 orders of magnitude smaller than the field, while the SA per year is only 1–2 orders of magnitude smaller than the SV. This failure of a steady flow to explain the full acceleration of the field has already been pointed out by others, e.g., *Waddington et al.* [1995], who found that a steady flow estimated directly from 30 years of observatory data failed to account for a significant portion of the change in the observed field [see also *Voorhies*, 1995].

3.2. Zonal Flow Acceleration

[22] A typical flow solution including terms for zonal acceleration is shown in Figure 5b. The corresponding flow velocity and acceleration spectra are shown in Figure 6b. It is seen from Figures 3 and 4 (green curve) that including zonal acceleration results in some improvement in explaining the observed SA while not significantly affecting the explained SV. This improvement is however marginal. Forcing the corresponding flow to better explain the SA by changing W_{SV} and W_{SA} is of course again possible. But it also again leads to a much poorer fit to the SV. This finally prompted us to look for a flow with a more general acceleration.

3.3. Generally Accelerated Flow

[23] Including the first time derivative of the flow doubles the number of unknown parameters. In order to reduce the number of unknowns, we allow only for toroidal flow, using the representations (7) and (8). As expected, an accelerated toroidal flow is able to simultaneously reproduce a large portion of the observed SV and SA (Figures 3 and 4, blue curves). However, its ability to explain the higher-degree SV and SA strongly depends on the applied damping. Here, we follow *Pais and Hulot* [2000] and *Eymin and Hulot* [2005] in imposing a rather strongly damped flow with a spectral decay rate of $p = 3$. Consequently, the solution only explains the low-degree portion of the observed SV and SA, to respectively about degrees 9 and 6. This, as we shall see

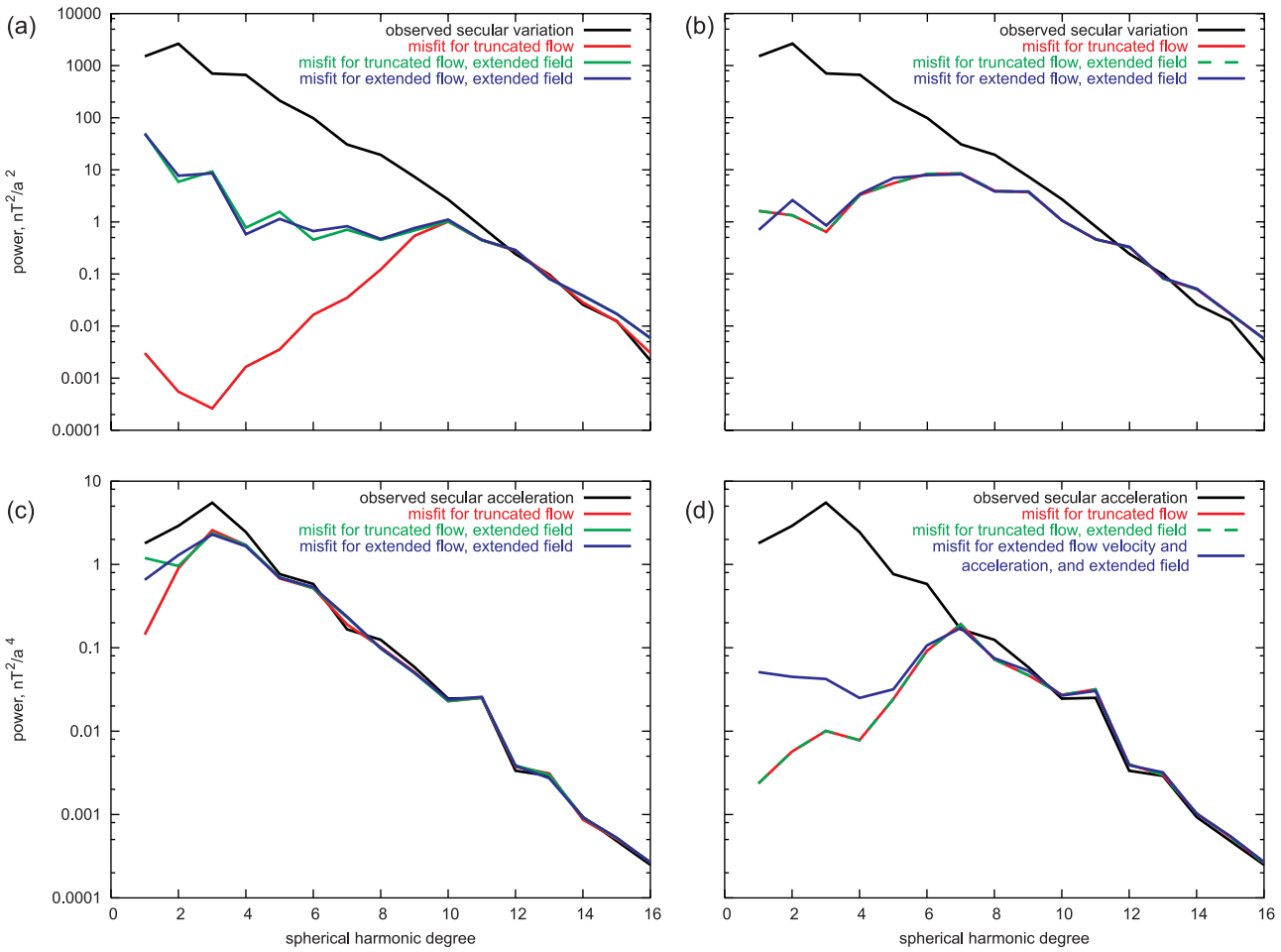

Figure 7. Results of testing the self-consistency of the flow solutions using random extensions of the main field, SV, flow velocity, and flow acceleration. (a) The SV (black curve) and the misfits between the modeled and the observed SV, for the recovered steady flow up to degree 16, interacting with the observed main field up to degree 13 (red curve); for the same flow interacting with the main field randomly extended up to degree 90 (green curve); and for the same flow randomly extended up to degree 40, interacting with main field randomly extended up to degree 90 (blue curve). (b) The same comparison for the generally accelerated toroidal flow. The analogous comparison for the SA for (c) the steady flow and (d) the generally accelerated toroidal flow, in the latter case both the flow itself and the flow acceleration being taken into account. All spectra are plotted at the Earth's surface.

next, is however not an issue. Such a level of misfit is that expected because of the requirement that the flow solution be self-consistent in the sense defined by *Eymin and Hulot* [2005]. The flow solution is shown in Figure 5c, while Figure 6c shows the flow velocity and acceleration spectra.

3.4. Self-Consistency of the Flow Solutions

[24] The tests of self-consistency for the steady and generally accelerated flow solutions are carried out in two steps (following lines similar to *Eymin and Hulot* [2005]):

[25] 1. The interaction of the truncated flow (and flow acceleration when relevant) with the unknown high-degree main field and SV results in additional unmodeled SV and SA. This unmodeled contribution adds to the misfit between the modeled and observed SV and SA. To estimate the magnitude of this effect, we randomly extend the observed main field and SV coefficients, scaled to maintain a constant decay of the field in single logarithmic scale (Figure 2). As seen in Figure 7 (green curves), this unmodeled contribution to the SV and SA is already significant

[26] 2. In a second step, contributions from the interaction of the randomly extended flow velocity and acceleration (Figure 6) are further taken into account (Figure 7, blue curves).

[27] Figure 7 then reveals that all contributions are comparable in magnitude to the observed SV and SA beyond respectively degrees 9 and 6, showing that the flow (and acceleration) should not attempt to directly account for the observed SV and SA beyond those degrees, as is indeed the case. This also shows that by contrast, all those contributions do not prevent the observed SV and SA below those degrees to be accounted for at a satisfying level. In summary, the interaction of the various high- and low-degree parts of the flow and the field make a significant (unknown) contribution to the observed SV and SA. However, if the true core flow has a spectrum decaying with an

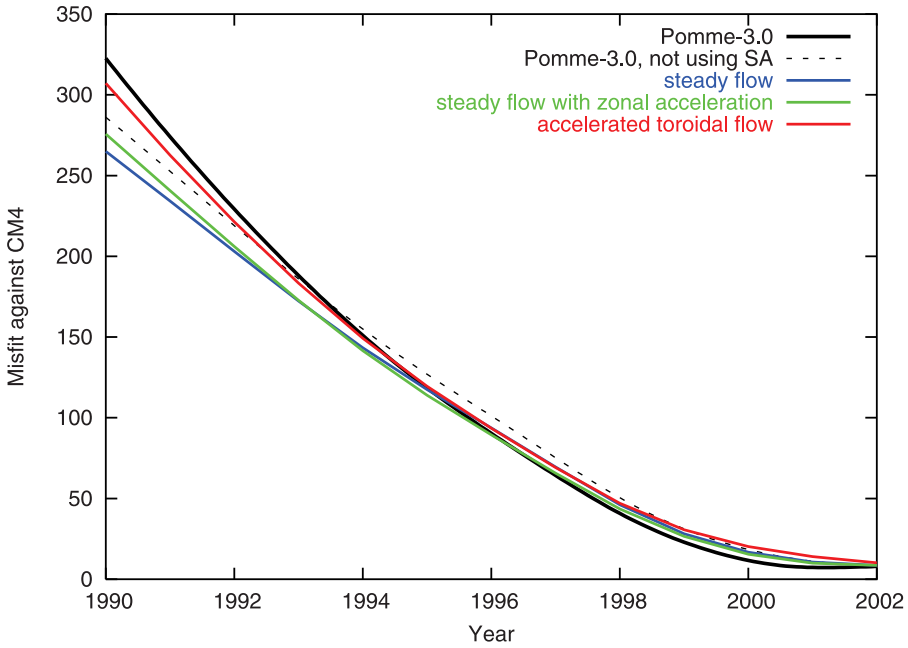

Figure 8. Misfit of the hindcast field with CM4 at the Earth's surface. All hindcasts are based directly, or indirectly via the inferred flow, on the Pomme-3.0 model which was estimated from data extending back to 2000.5, while CM4 is based on data extending back to 1960. The lowest misfit is achieved for a steady flow.

exponent of $p \geq 3$, this contribution is found to be small in comparison with the total SV and SA at low degrees. Our $p = 3$ solutions can thus be considered as self-consistent (in the sense defined by *Eymin and Hulot* [2005]).

3.5. Hindcast of the Geomagnetic Field

[28] We wish to test the possibility of forecasting the main field by representing its temporal evolution in terms of core flow. However, accurate models of the SV and SA have not yet been available for long enough to allow for such a direct test. Here we therefore choose to assess the accuracy of a hindcast based on the same approach, which we test by comparison with the past geomagnetic field, as given by the Comprehensive Model [*Sabaka et al.*, 2004], the domain of validity of which extends from 1960 to 2002. The procedure is the following. Consider a pair of flow and flow acceleration estimates computed as described in the previous section for the t_0 = 2003.0 reference epoch of the POMME3.0 model. Denote those estimates u_0 and $\dot{u}_0$. Then the hindcast is done in time steps of δt by the following recursive scheme: (1) start at $t = t_0 = 2003.0$, with $g_\ell^m(t) = g_\ell^m(t_0)$ and $u(t) = u(t_0) = u_0$; (2) predict $\dot{g}_\ell^m(t)$ up to degree 13 using equation (2) (without the diffusion term, of course); (3) update $g_\ell^m(t - \delta t) = g_\ell^m(t) - \delta t \dot{g}_\ell^m(t)$. This is the field hindcast for $t - \delta t$; (4) to account for flow acceleration $\dot{u}_0$ (assumed constant throughout the hindcast period), update the flow by $u(t - \delta t) = u(t) - \delta t \dot{u}_0$; (5) update the time $t_{new} = t_{old} - \delta t$; and (6) go to step 2. The smaller the time step, the more accurate the scheme. In practice, since the flow acceleration is rather weak, a time step of 1 year was found to be sufficiently small to track the changes accurately.

[29] The difference between the predicted field and the Comprehensive Model (CM4) at the Earth's surface is then computed as the cumulative Mauersberger/Lowes spectrum, added up over all degrees as

$$dP = \sum_{\ell=1}^{N} \sum_{m=-\ell}^{\ell} (\ell + 1) \left((g_\ell^m)_{predicted} - (g_\ell^m)_{CM4} \right)^2. \qquad (16)$$

Here, $\sqrt{dP}$ is identical to the root mean square (RMS) difference between the two fields at the Earth's surface. This RMS difference between hindcast and CM4 is shown in Figure 8 for our three different flow parameterizations. Also shown are the results from two simple hindcastings methods, which we will use for reference to measure the possible improvement brought by core flow based hindcasts. The first method simply consists in making use of POMME3.0 (including its SA), to extrapolate the field backward. The second consists in using the same model POMME3.0 but assuming no SA at all. We will discuss Figure 8 in the next section.

4. Discussion and Conclusion

[30] This study was motivated by the desire to test whether representing magnetic field secular change in terms of its physical cause, namely core-surface flow, could result in a more accurate prediction of the magnetic field for a time span of 5–10 years. In implementing such a representation, we however faced two major obstacles: The first concerns the truncation of the observable main field and SV at rather low degrees, namely 13 and 16, respectively. If the true core-surface flow spectrum decreases with an exponent close to $p = 1$ (the energetic lower limit for p), the various interactions of the high-degree main field, SV, flow velocity and flow acceleration are most likely to make a significant

contribution to the observed SV and SA, even at the lowest degrees. Since these effects cannot be modeled, because of the unknown high-degree field, the true core-surface flow would then be impossible to determine (an issue, we know from dynamo simulations, can cause serious problems, as is discussed by, e.g., *Rau et al.* [2000]). On the other hand, if the large-scale SV is predominantly caused by large-scale flow, then it is rather straightforward to invert for the most likely flow, especially if the true spectrum of the flow velocity and its acceleration decay rapidly, with $p \geq 3$ as we have assumed. This is a fairly strong assumption, but the success of flow models at hindcasting the geomagnetic field will eventually provide some indication of the relevance of this assumption, at least for hindcasting and forecasting purposes.

[31] The second difficulty is that a steady flow fails to simultaneously explain the SV and SA, the latter being too strong. This problem had previously been noted by others [e.g., *Bloxham and Jackson*, 1991; *Hulot et al.*, 1993; *Waddington et al.*, 1995]. Consequently, a complete representation of the magnetic secular change in terms of core-surface flow must include flow acceleration, adding a large number of degrees of freedom to the flow model. The challenge is then to impose physically reasonable constraints on the solution in order to reduce the ambiguity of the inverse problem. Here, we chose to limit the solution to be a toroidal flow. Then indeed, the resulting flow solution does explain the low-degree SA in addition to the SV. Now, what about the hindcasting success of such flows?

[32] First consider the success of the first reference hindcasting method (on the basis of the POMME3.0 model itself). This method leads to an almost constant very low misfit over the 2000.5–2002 time period (Figure 8). This hardly is a surprise since both POMME3.0 and CM4 have been built to account for observations carried out over that period of time (see *Maus et al.* [2006]; *Sabaka et al.* [2004]; *Hulot et al.* [2007] for more details). This short-term hindcasting success thus only gives a measure of the accuracy with which such models can account for the main field evolution over their overlapping domains of validity. But it can also be viewed as a measure of the least possible misfit one can expect when truly hindcasting (or forecasting) the main field. Indeed, before 2000.5, hindcasts from POMME3.0 lead to a larger misfit, increasing with the distance from epoch 2000.5.

[33] Next, consider the success of the second reference method (POMME3.0 without taking the SA into account). Not surprisingly, this leads to a slightly worse misfit over the 2000.5–2002 time period (confirming the need for POMME3.0 to include a SA over its domain of validity). But as one moves back in time, the situation changes and before 1994, this second method eventually turns out to be better than the previous one. This interesting result simply shows that the POMME3.0 SA, which is tuned to describe the 2000.5 to 2005.5 time period, is not adequate for earlier epochs, and that the average SA over the 1990–2002 time period is closer to zero. This, in fact, should not come as a surprise, since it is known that several jerks occurred since 1990 (in 1996, 1999 and 2003 [see, e.g., *Olsen and Mandea*, 2007]) and that jerks correspond to sudden changes in the SA [e.g., *Courtillot et al.*, 1978] that tend to cancel each other on the long term [*Alexandrescu et al.*, 1996; *Le Huy et al.*, 1998].

[34] What about core flow based hindcasts? Figure 8 shows that overall (and even for short-term hindcasts, although quite marginally so), the worst hindcast is provided by the accelerated toroidal flow, a hindcast of intermediate quality is provided by the steady flow with zonal acceleration, and the best hindcast is provided by the steady flow, the difference in hindcasting performances becoming larger as one moves away from 2002. The ranking of those flows in terms of hindcasting thus appears to be just the opposite of their ranking in terms of their ability to account for the POMME3.0 SA (recall Figure 4). Those interesting results can again be understood in terms of the nonstationary nature of the SA. Hindcasts based on the core flows that best account for the POMME3.0 SA implicitly make the assumption that the flow acceleration explaining this SA has been stationary throughout the hindcasting time period. But just like the SA itself, flow acceleration is known not to be stationary over long time periods and to in fact change faster than the flow itself. First, because at least in the present conceptual frozen flux framework, sudden changes of SA at times of jerks necessarily imply sudden changes in flow acceleration [see, e.g., *Le Huy et al.*, 1998], and second, because length of day variations on decade timescales also require such accelerations in the zonal component of the flow [*Jault et al.*, 1988]. It thus follows that an estimate of the flow acceleration based on a short-term SA estimate cannot be used to improve hindcasts, at least when considering a time period involving several jerks (which then tend to average out not only the SA, but also the flow accelerations, [*Le Huy et al.*, 1998]).

[35] However, and most interestingly, it also appears that except when considering relatively short-term hindcasts (say back to 1996, when the reference hindcast based on the full POMME3.0 model does best, though not so much so), the best method turns out to be the one based on the steady flow, which does significantly better than the best of the two reference methods (POMME3.0 without any SA). This result has two implications for forecasting provided, of course, one may extrapolate the present hindcasting results to forecasting. One is that forecasts based on core flow calculations could indeed prove more efficient than forecasts based on a Taylor expansion type of extrapolation of a field model. The other is that, in absence of a better understanding of the exact dynamical nature of geomagnetic jerks and while waiting for more elaborate data assimilation type procedures (on the basis of the works of, e.g., *Fournier et al.* [2007], or *Liu et al.* [2007]), medium-term forecasts (beyond several jerks) might prove easier to achieve than short-term forecasts (between jerks), by just relying on a stationary flow estimate. With this respect, additional tests analogous to those reported here, over periods of time when no jerks occured, such as between 1971 and 1979, could prove useful. This however, is beyond the scope of the present study because no high-quality SA model independent of CM4 (such as POMME 3.0) is currently available for such earlier epochs. It is nevertheless our opinion that core flow based forecasts should further be considered and investigated.

[36] **Acknowledgments.** We thank Nils Olsen and three anonymous reviewers for their valuable comments on earlier versions of the manuscript.

S.M. is grateful for the invitation to IPGP, where this collaborative work was carried out. This is IPGP contribution 2381.

References

Alexandrescu, M., C. H. Duyen, and J.-L. LeMouël (1994), Geographical distribution of magnetic observatories and field modeling, *J. Geomagn. Geoelectr.*, *46*, 891–901.

Alexandrescu, M., D. Gibert, G. Hulot, J.-L. LeMouël, and G. Saracco (1996), Worldwide wavelet analysis of geomagnetic jerks, *J. Geophys. Res.*, *101*, 21,975–21,994.

Alexandrescu, M. M., D. Gibert, J.-L. LeMouël, G. Hulot, and G. Saracco (1999), An estimate of average lower mantle conductivity by wavelet analysis of geomagnetic jerks, *J. Geophys. Res.*, *104*, 17,735–17,745.

Backus, G., R. L. Parker, and C. Constable (1996), *Foundations of Geomagnetism*, Cambridge Univ. Press, New York.

Backus, G. E. (1968), Kinematics of geomagnetic secular variation in a perfectly conducting core, *Philos. Trans. R. Soc. London Ser. A*, *263*, 239–266.

Bloxham, J., and A. Jackson (1991), Fluid flow near the surface of the Earth's outer core, *Rev. Geophys.*, *29*(1), 97–120.

Bloxham, J., and A. Jackson (1992), Time-dependent mapping of the magnetic field at the core-mantle boundary, *J. Geophys. Res.*, *97*, 19,537–19,563.

Bloxham, J., S. Zatman, and M. Dumberry (2002), The origin of geomagnetic jerks, *Nature*, *420*, 65–68.

Braginsky, S. I. (1970), Torsional magnetohydrodynamics vibrations in the Earth's core and variations in day length, *Geomagn. Aeron.*, *10*, 3–12.

Courtillot, V., J. Ducruix, and J.-L. LeMouël (1978), Sur une acceélération récente de la variation séculaire du champ magnétique terrestre, *C.R. Acad. Sci. Ser. D*, *287*, 1095–1098.

Eymin, C., and G. Hulot (2005), On core surface flows inferred from satellite magnetic data, *Phys. Earth Planet. Inter.*, *152*, 200–220.

Fournier, A., C. Eymin, and T. Alboussière (2007), A case for variational geomagnetic data assimilation: Insights from a one-dimensional, nonlinear, and sparsely observed MHD system, *Nonlinear Processes Geophys.*, *14*, 163–180.

Gubbins, D., and J. Bloxham (1985), Geomagnetic field analysis– Part III. Magnetic fields on the core-mantle boundary, *Geophys. J. R. Astr. Soc.*, *80*, 695–713.

Holme, R. (1998), Electromagnetic core-mantle coupling I. Explaining decadal changes in the length of day, *Geophys. J. Int.*, *132*(1), 167–180.

Holme, R., and N. Olsen (2006), Core surface flow modelling from high-resolution secular variation, *Geophys. J. Int.*, *166*, 518–528.

Hulot, G., J. L. LeMouël, and J. Wahr (1992), Taking into account truncation problems and geomagnetic model accuracy in assessing computed flows at the core-mantle boundary, *Geophys. J. Int.*, *108*, 224–246.

Hulot, G., M. L. Huy, and J.-L. LeMouël (1993), Secousses (jerks) de la variation séculaire et mouvements dans le noyau terrestre, *C. R. Acad. Sci. Ser. II*, *317*, 333–341.

Hulot, G., C. Eymin, B. Langlais, M. Mandea, and N. Olsen (2002), Small-scale structure of the geodynamo inferred from Ørsted and Magsat satellite data, *Nature*, *416*, 620–623.

Hulot, G., T. Sabaka, and N. Olsen (2007), The present field, in *Geomagnetism*, *Treatise Geophys.*, vol. 5, edited by G. Schubert, pp. 33–75, Elsevier, New York.

Jackson, A. (1997), Time-dependency of tangentially geostrophic core surface motions, *Phys. Earth Planet. Inter.*, *103*, 293–311.

Jackson, A., and C. Finlay (2007), Geomagnetic secular variation and its applications to the core, in *Geomagnetism*, *Treatise Geophys.*, vol .5, edited by G. Schubert, pp. 147–193, Elsevier, New York.

Jault, D., C. Gire, and J.-L. LeMouël (1988), Westward drift, core motions and exchanges of angular momentum between core and mantle, *Nature*, *333*, 353–356.

Jault, D., G. Hulot, and J.-L. LeMouël (1996), Mechanical core-mantle coupling and dynamo modelling, *Phys. Earth Planet. Inter.*, *98*, 187–192.

Langel, R. A., and W. J. Hinze (1998), *The Magnetic Field of the Earth's Lithosphere—The Satellite Perspective*, Cambridge Univ. Press, New York.

Le Huy, M., M. Alexandrescu, G. Hulot, and J.-L. LeMouël (1998), On the characteristics of successive geomagnetic jerks, *Earth Planets Space*, *50*, 723–732.

LeMouël, J.-L. (1984), Outer core geostrophic flow and secular variation of Earth's magnetic field, *Nature*, *311*, 734–735.

Liu, D., A. Tangborn, and W. Kuang (2007), Observing system simulation experiments in geomagnetic data assimilation, *J. Geophys. Res.*, *112*, B08103, doi:10.1029/2006JB004691.

Maus, S., S. Macmillan, F. Lowes, and T. Bondar (2005a), Evaluation of candidate geomagnetic field models for the 10th generation of IGRF, *Earth Planets Space*, *57*, 1173–1181.

Maus, S., et al. (2005b), The 10th-generation International Geomagnetic Reference Field, *Geophys. J. Int.*, *161*, 561–565, doi:10.1111/j.1365-246X.2005.02641.x..

Maus, S., M. Rother, C. Stolle, W. Mai, S. Choi, H. Lühr, D. Cooke, and C. Roth (2006), Third generation of the Potsdam Magnetic Model of the Earth (POMME), *Geochem. Geophys. Geosyst.*, *7*, Q07008, doi:10.1029/2006GC001269.

McLean, S., S. Macmillan, S. Maus, V. Lesur, A. Thomson, and D. Dater (2004), The US/UK World Magnetic Model for 2005–2010, *Tech. Rep. NESDIS/NGDC-1*, NOAA, Boulder, Colo.

Menke, W. (1984), *Geophysical Data Analysis: Discrete Inverse Theory*, Academic, New York.

Mound, J., and B. Buffett (2005), Mechanisms of core-mantle angular momentum exchange and the observed spectral properties of torsional oscillations, *J. Geophys. Res.*, *110*, B08103, doi:10.1029/2004JB003555.

Olsen, N., and M. Mandea (2007), Investigation of a secular variation impulse using satellite data: The 2003 geomagnetic jerk, *Earth Planet. Sci. Lett.*, *225*, 94–105.

Olsen, N., H. Lühr, T. J. Sabaka, M. Mandea, M. Rother, L. Tøffner-Clausen, and S. Choi (2006), CHAOS—A model of Earth's magnetic field derived from CHAMP, Ørsted, and SAC-C magnetic satellite data, *Geophys. J. Int.*, *166*, 67–75, doi:10.1111/j.1365-246X.2006.02959.x.

Pais, A., and G. Hulot (2000), Length of day decade variations, torsional oscillations and inner core superrotation: Evidence from recovered core surface zonal flows, *Phys. Earth Planet. Inter.*, *118*, 291–316.

Rau, S., U. Christensen, A. Jackson, and J. Wicht (2000), Core flow inversion tested with numerical dynamo models, *Geophys. J. Int.*, *141*, 485–497.

Roberts, P., and S. Scott (1965), On analysis of the secular variation, *J. Geomagn. Geoelectr.*, *17*, 137–151.

Sabaka, T. J., N. Olsen, and M. E. Purucker (2004), Extending comprehensive models of the Earth's magnetic field with Ørsted and CHAMP data, *Geophys. J. Int.*, *159*, 521–547, doi:10.1111/j.1365-246X.2004.02421.x.

Voorhies, C. (1995), Time-varying fluid flow at the top of the Earth's core derived from definitive geomagnetic reference field models, *J. Geophys. Res.*, *100*(B7), 10,029–10,039.

Voorhies, C. (2004), Narrow-scale flow and a weak field by the top of the Earth's core: Evidence from Ørsted, Magsat, and secular variation, *J. Geophys. Res.*, *109*, B03106, doi:10.1029/2003JB002833.

Voorhies, C., and G. Backus (1985), Steady flows at the top of the core from geomagnetic field models: The steady motions theorem, *Geophys. Astrophys. Fluid Dyn.*, *32*, 163–175.

Waddington, R., D. Gubbins, and N. Barber (1995), Geomagnetic field analysis—Part V. Determining steady core-surface flows directly from gomagnetic observations, *Geophys. J. Int.*, *122*, 326–350.

Whaler, K. A. (1980), Does the whole of the Earth's core convect, *Nature*, *287*, 528–530.

Zatman, S., and J. Bloxham (1999), On the dynamical implications of models of B_s in the Earth's core, *Geophys. J. Int.*, *138*, 679–686.

G. Hulot and L. Silva, Equipe de Géomagnétisme, Institut de Physique du Globe de Paris, INSU/CNRS, Université Paris Diderot, Boîte Postale 89, 4 place Jussieu, F-75252 Paris CEDEX 05, France.

S. Maus, National Geophysical Data Center, NOAA E/GC1, 325 Broadway, Boulder, CO 80305-3328, USA. (stefan.maus@noaa.gov)